Magnetism and the defect state in the magnetocaloric antiperovskite $Mn_3GaC_{1-\delta}$

Magnetism and the defect state in the magnetocaloric antiperovskite $Mn_3GaC_{1-\delta}$

L H Lewis[1], D Yoder[2,3], A R Moodenbaugh[1], D A Fischer[2] and M-H Yu[1,4]

[1] Materials Science Department, Building 480, Brookhaven National Laboratory, Upton, NY 11973-5000, USA
[2] Materials Science and Engineering Laboratory, National Institute of Standards and Technology, Gaithersburg, MD 20899, USA

E-mail: LHLewis@bnl.gov

Abstract

Magnetic and spectroscopic techniques were used to study the intermetallic antiperovskite Mn_3GaC. An antiferromagnetic–ferromagnetic magnetostructural transition at 160 K underlies a remarkable magnetocaloric effect; these phenomena are suppressed in the substoichiometric composition $Mn_3GaC_{1-\delta}$. X-ray absorption spectroscopy (XAS) data reported for three compositions $Mn_3GaC_{1-\delta}$, $\delta = 0, 0.10, 0.22$, are the basis for drawing inferences concerning the mechanism controlling magnetic order as a function of carbon stoichiometry. While the temperature dependence of the Mn_3GaC carbon K edge reveals no observable change across the first-order magnetic transition, a clear splitting of the carbon absorption bands is observed that increases with increasing carbon deficiency. The room temperature Mn and Ga K edges indicate no significant variation with C content. FEFF 8.2 code calculations are in good qualitative agreement with data for the stoichiometric sample, but do not predict the changes in XAS observed in C-deficient samples. These results and the Goodenough–Anderson–Kanamori rules are the basis for a phenomenological model that attributes the carbon content dependence of the low temperature transition to the promotion of weak near-neighbour 90° Mn–Mn pairs in the carbon-deficient compound over the stronger 180° Mn–C–Mn interaction, locking in dominant ferromagnetism at low temperatures.

[3] Present address: GM/CA-CAT, Building 436D, Argonne National Laboratory, 9700 S. Cass Avenue, Argonne, IL 60439, USA.
[4] Present address: Advanced Materials Research Institute, University of New Orleans, New Orleans, LA 70148, USA.

1. Introduction

The intermetallic antiperovskite compound Mn_3GaC is a member of an intriguing class of materials that undergo a first-order magnetic transition (FOMT) that may be driven by temperature T, pressure or magnetic field H and are characterized by the simultaneous occurrence of a magnetic and a structural transition. The magnetization profile of the transition exhibits a discontinuous change with T that implies highly correlated coupling between the magnetic spins and the lattice. FOMTs are recognized as the source of extraordinary functional phenomena, including colossal magnetoresistance (CMR) found in the manganites [1] and the giant magnetocaloric effect (MCE) found in $Gd_5(Si_{1-x}Ge_x)_4$ [2]. The extraordinary mechanical behaviour of the FM shape memory alloy Ni_2MnGa [3] is also related to a FOMT.

Here synchrotron-based x-ray absorption spectroscopy (XAS) is employed to investigate relations among stoichiometry, bonding, and the magnetic state of the antiperovskite compound $Mn_3GaC_{1-\delta}$, $\delta = 0$, 0.10, 0.22. In its stoichiometric form, Mn_3GaC exhibits, on increasing temperature through $T = 160$ K, an abrupt transformation from antiferromagnetism (AFM) to ferromagnetism (FM) with an associated volume contraction that underlies the magnetic entropy change of 13.7 J kg^{-1} K^{-1} in $H = 1$ T. This entropy change produces a magnetocaloric effect that is markedly larger than that of the prototypical MCE material $GdAl_2$, 7.6 J^{-1} kg^{-1} K^{-1}, under the influence of a field $H = 5$ T in the same temperature range [4].

In contrast to Mn_3GaC, the carbon-deficient $Mn_3GaC_{1-\delta}$ retains the FM state to lowest measured temperatures. This feature is reminiscent of the recent report that superconductivity in the isostructural carbide Ni_3MgC_{1-x} is suppressed to lower temperatures as x is increased [5]. Despite the very pronounced differences in magnetic properties, x-ray diffraction shows only a slight variation of lattice parameter. The mechanism and driving force underlying the distortion remain unclear, despite an appreciable amount of experimental and computation work devoted to this compound. Thus XAS investigations were carried out on the K absorption edges of manganese, gallium, and carbon in $Mn_3GaC_{1-\delta}$ to clarify the origins of the transition. The results reveal systematic changes with stoichiometry in the unoccupied states above the carbon valence band that are analysed to provide a phenomenological description of the FOMT driving force in Mn_3GaC.

Cubic (space group $Pm3m$) Mn_3GaC, first reported in 1957 [6], was later observed to exhibit unusual magnetic properties as well as a unique relationship between its defect structure and its magnetic character [7–9]. The Ga atom sits on cubic lattice sites with the Mn and the C atoms located at the face-centred and body-centred positions, respectively. With increasing T, Mn_3GaC exhibits a FOMT from an AFM to a canted FM (CFM) phase at ∼160 K [8, 10] accompanied by a discontinuous volume change of −0.46% without change of crystal structure [11]. One second-order phase transformation from CFM to collinear FM occurs at $T \sim 164$ K while another second-order transformation from collinear FM to paramagnetic (PM) takes place at the Curie temperature $T_C \sim 249$ K [10]. In the AFM and FM phases, the Mn cations carry the moment which resides in a given (111) plane, uniform along a [111] direction, with values on the order of 1.8 μ_B/Mn atom in the AF state and 1.2 μ_B/Mn atom in the FM state [12, 13]. This reduction in Mn moment that accompanies the unit cell contraction is thought to be associated with a stronger Mn metallic 3d orbital overlap that broadens the d band. These moments are smaller than those expected in compounds with localized Mn cations (∼5 μ_B/Mn) confirming dominant itinerant electronic character. The extremely abrupt magnetization change in the FOMT AFM–CFM transition (it can reach ∼70 A m^2 kg^{-1} (70 emu g^{-1})) [11] underlies the large MCE effect found in Mn_3GaC near the AFM–CFM phase transition temperature T_t [4] and is also the origin of the giant magnetoresistance found in the same temperature region [14, 15].

The AFM–CFM T_t in Mn_3GaC is dependent upon the magnitude of the magnetic field applied during measurement [8, 10, 11] and, to a much greater degree, on the carbon stoichiometry. Bouchaud and Fruchart [7] found that T_t is depressed with carbon deficiency, and at $\delta = 0.04$, the compound is FM down to lowest temperature. The application of pressure, either by chemical [16, 17] or physical means [9, 10, 18, 19], also changes the nature of the magnetic transitions in the Mn_3GaC. It is reported that the FOMT temperature decreases while that of the second-order magnetic transition temperature increases with increasing pressure, implying stabilization of the FM state with pressure. This result is unusual among itinerant systems. Increased pressure, which reduces interatomic distances, is expected to increase the bandwidth, resulting not only in a reduced Mn moment but also a lower T_c [16, 20].

Results obtained on other metallic compounds provide guidance concerning the nature of the electronic interactions in Mn_3GaC. The application of pressure induces AFM nearest-neighbour Fe–Fe interactions in fcc Fe–Ni alloys for 30–50 at.% Ni, thereby producing an increase in T_c [21]. As a similar mechanism may be operative in $Mn_3GaC_{1-\delta}$, it is important to correlate the composition-dependent atomic environment with the magnetic state. In this paper we probe the local atomic environment using XAS, a technique that reveals the electronic structure of element-specific unoccupied states above the Fermi level, and, hence, their bonding character. Samples are exposed to tunable, monochromatic x-ray radiation from a synchrotron light source. The absorption spectra are then obtained by collecting byproducts of the relaxation process, either the characteristic Auger electrons (electron yield) or fluorescent photons (fluorescence yield). Computational modelling of the data usually provides qualitative or semiquantitative accuracy. Here, FEFF 8.2 [22], which incorporates a self-consistent calculation of atomic potentials and a full multiple scattering calculation for improved near-edge treatment, is used to model both the near-edge and extended absorption data. Absorption spectra for the carbon K edge for the three compositions of $Mn_3GaC_{1-\delta}$ will be displayed and analysed. Additional spectra for manganese, and gallium K edges, as well as at the manganese and gallium L_{III}/L_{II} edges, will be briefly described.

2. Synthesis and phase characterization

A polycrystalline sample of $Mn_3GaC_{1-\delta}$ was prepared by a direct reaction of the elements as described in [4]. The initial product was deficient in carbon, with composition estimated to be $Mn_3GaC_{0.78}$ on the basis of x-ray diffraction and helium pycnometer density measurements. Additionally, magnetic assessment was consistent with substoichiometric material, showing a pure FM state for $T > 5$ K, with a Curie point $T_c \sim 295$ K. One part of this $\delta = 0.22$ (formula carbon 0.78) sample was reserved for further study. The remainder was divided into two portions. Each was ground together with additional carbon, one with 0.12 formula to synthesize $Mn_3GaC_{0.90}$, the other with 0.22 formula carbon to synthesize Mn_3GaC. These powders were pressed into pellets, sealed in silica under an inert atmosphere, and heated at 1073 K for another seven days. After this procedure, the nominally stoichiometric Mn_3GaC revealed the characteristic AFM–FM $T_t \sim 160$ K. According to x-ray diffraction using Cu Kα radiation, Mn_3GaC is cubic and single phase. The lattice parameter $a = 3.8942(7)$ Å was determined by a least-squares fit of the Bragg peak positions and is in agreement with [7]. The other two samples retain cubic symmetry and have lattice parameters: $Mn_3GaC_{0.90}$, $a = 3.8942(6)$ Å; $Mn_3GaC_{0.78}$, $a = 3.8851(7)$ Å.

Magnetic assessment of the carbon-deficient compound $Mn_3GaC_{0.78}$ with a Quantum Design MPMS SQUID magnetometer indicated a total collapse of the AFM state, producing a pure FM state from $T = 5$ K with a $T_C = 295$ K (figure 1). The T dependences of the magnetization of Mn_3GaC and $Mn_3GaC_{0.78}$ at applied fields of 10 and 100 mT are shown in
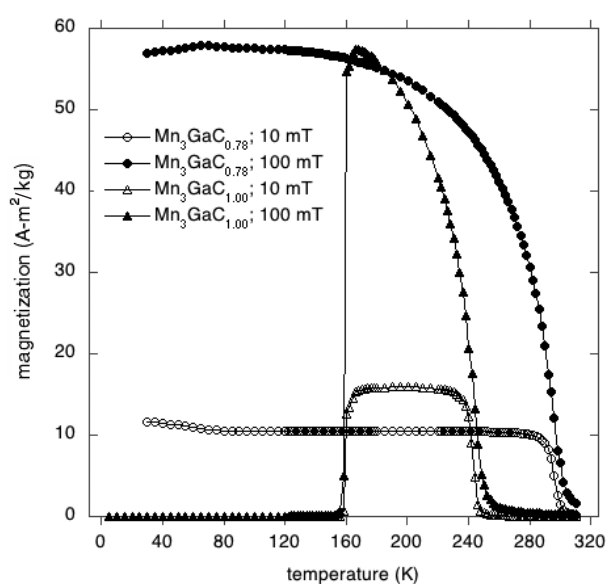
Figure 1. Temperature dependence of the magnetization of nominally stoichiometric Mn_3GaC and the substoichiometric $Mn_3GaC_{0.78}$ compounds at applied fields of 10 and 100 mT.

figure 1. While earlier literature [7, 23] reported the collapse of the AFM state in $Mn_3GaC_{1-\delta}$ at carbon deficiencies of 4 at.%, in this study little difference in the magnetic character of $Mn_3GaC_{0.90}$ and $Mn_3GaC_{1.0}$ as observed. In stoichiometric Mn_3GaC, the FOMT (AFM to canted FM (CFM)) occurs at $T_{cr1} = 159$ K with the CFM phase transforming via a second-order transition to a collinear FM phase at $T_{cr2} = 165$ K. Increasing the measuring field does not broaden the abrupt transition between AFM and CFM phases. The Curie temperature T_C was taken to be the temperature of the maximum temperature derivative of the magnetization measured at $\mu_0 H = 10$ mT to yield $T_C = 245$ K. These results are comparable to those obtained in [10]. The temperature hysteresis of the first-order AFM to CFM phase transition is finite but small with $\Delta T = 2$ K.

3. X-ray absorption measurements

XAS measurements were conducted at the National Synchrotron Light Source at Brookhaven National Laboratory. This paper emphasizes results for the C K edge obtained at beamline U7A. For these data, monochromatic radiation is provided via a 600 line mm^{-1} grating. Near-edge XAS (NEXAFS) data were obtained in the NIST-Dow materials characterization chamber operating at a pressure of 1.3×10^{-5} Pa (10^{-8} Torr). Supplemental XAS data were obtained at beamline U7A for the Mn and Ga L_{III}/L_{II} edges and at beamline X11B for the Mn and Ga K edges. Previously published Mn K data, along with x-ray magnetic circular dichroism data, are published in [24]. Because these supplemental data are only briefly described, the experimental conditions will not be documented here.

For the C K edge, the monochromator energy was calibrated to the π^* absorption of graphite at the carbon K edge (285.35 eV). The energy resolution near the C K edge is estimated to be 0.1 eV and the energy step size near the edge jump was 0.1 eV. Spectra were collected as fluorescence yield using a solid state detector. Individual data points were normalized to the
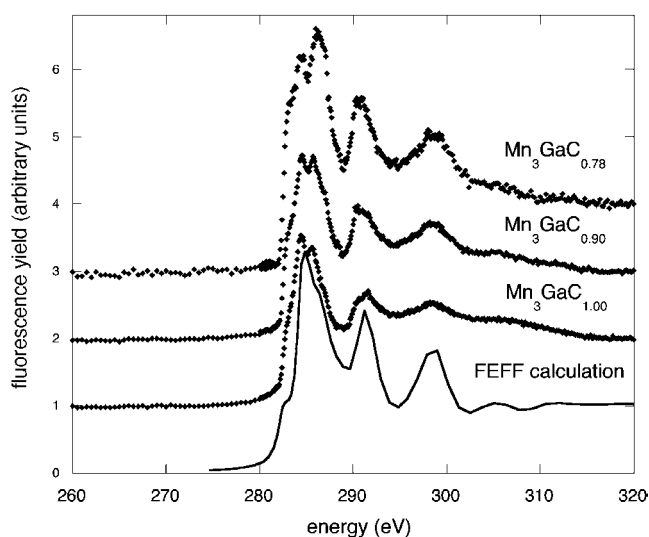
Figure 2. Room temperature carbon NEXAFS data measured for the three samples displayed with the fit to the data using the FEFF calculation. Data are offset vertically for clarity of presentation.

incident beam intensity (I_0) on the basis of the total electron yield from a gold-coated 90% transmitting grid placed in the x-ray beam path. Each spectrum was then normalized to an edge jump of unity, on the basis of the observed intensity near 320 eV. While most of the data were taken at room temperature, Mn$_3$GaC was also cooled on a nitrogen cold finger in the evacuated experimental chamber to obtain an additional set of carbon K edge data below $T_t = 160$ K.

Simulations of the carbon K edge features were performed with FEFF 8.2. Calculations converged utilizing a $\sim$150 atom cluster representing $\sim$30 unit cells of Mn$_3$GaC. The manganese K edge XAS data were analysed [25] and fit with theoretical phase and amplitude functions obtained from FEFF 8.2.

The room temperature carbon NEXAFS data are displayed in figure 2. Carbon K edge NEXAFS reflects primarily the carbon bonding to the Mn, and may be less sensitive to the phase transition and associated details of the Mn magnetic state. However, as the unit cell volume at room temperature and at 125 K differ only by 0.05% [26], after recovery from the rapid drop at $T = 160$ K upon heating, this result may be expected. Moreover, the spectrum of Mn$_3$GaC is marked by the edge jump just below $E = 285$ eV and weaker resonances at 291 and 298 eV. The spectral differences between stoichiometric Mn$_3$GaC and lower carbon compositions can be most readily observed in the 286–287 eV region. A transition in Mn$_3$GaC represented by a peak at 285.6 eV appears to increase in intensity and shift to $\sim$285.9 eV for Mn$_3$GaC$_{0.78}$. An additional feature at 286.5 eV, negligible in Mn$_3$GaC, becomes noticeable in Mn$_3$GaC$_{0.90}$ and prominent in Mn$_3$GaC$_{0.78}$. Further, a third minor transition appears just above the Fermi level at 283 eV. Additional features appear at higher energies, 290.5 and 298 eV. There was no significant change in the carbon NEXAFS spectrum of Mn$_3$GaC observed at $T \sim 125$ K (below $T_t = 160$) from that at room temperature.

The invariance of the metal K edges with carbon content suggests that the number of electrons delocalized from the metal atoms does not vary strongly with C deficiency. Rather, these electrons are hypothesized to shift from bonding with carbon to occupying the conduction band as carbon is removed. In contrast to obvious differences among the spectra at the carbon edge, the near-edge spectra of Mn and Ga (at both the K and L edges) for the various

stoichiometries reveal no significant differences above the level of uncertainty (data not shown). These results imply that Mn and Ga do not participate in driving the transition.

The carbon K NEXAFS spectroscopy data were modelled using FEFF 8.2. FEFF is an automated program for *ab initio* higher order multiple scattering calculations of x-ray absorption fine structure (XAFS) and x-ray absorption near-edge structure (XANES) spectra for atomic clusters. The model aims to fit the weak oscillatory signal at energies greater than the absorption edge by modelling them as quantum-interference phenomena of electron waves that either constructively or destructively interact at the absorbing atom [27]. The model employed to fit the extended x-ray absorption fine structure (EXAFS) data resulting from the XAS of the Mn and Ga K edges allowed crystallographic $Mn_3GaC_{1-\delta}$ unit cell size to vary, while constraining the carbon coordination numbers to those determined from diffraction and helium pycnometer density methods (see above). On the basis of this model, the EXAFS-derived cubic lattice parameter shows the expected trend, decreasing from 3.87 Å in the stoichiometric compound to 3.81 Å in $Mn_3GaC_{0.78}$. Although the value of the lattice parameters derived from EXAFS data for the carbon-deficient compound differs from those determined by diffraction, possibly due to the presence of an impurity phase detected by EXAFS but not by XRD, the trend of reduced lattice parameter with reduced carbon content is preserved. It must also be noted that, during a preliminary survey scan over a broad energy range, all samples exhibited a significant oxygen K absorption edge. However, no changes in the oxygen near-edge spectra were observed with changing carbon content, and no XRD Bragg peaks corresponding to oxide phases were observed. Therefore it is assumed that the oxygen is sequestered in magnetically inert, poorly formed phases residing in intergranular regions and is not contributing to the observed magnetostructural phenomena in $Mn_3GaC_{1-\delta}$.

The initial input assumed a cluster of 150 atoms with $a = 3.894$ Å representing the full stoichiometric lattice. In addition, the calculation included a 1.0 eV shift in the Fermi level and instrumental broadening of 0.5 eV. Although FEFF does not necessarily provide accurate estimates of the absolute energies of the various edge transitions (the final calculations are shifted by ~ 8 eV) [27], the calculations of the relative energies are quite good. Major peaks as well as smaller features are well described, with relative calculated energies within 1 eV of the observed values (figure 2). FEFF predicts three features within ~ 3 eV of the Fermi level for the stoichiometric compound. These correspond well to a minor peak near 283 eV, a major peak near 285 eV, and a minor peak near 286 eV. In addition, the FEFF calculations are qualitatively consistent with the C 2p band structure calculations of Mn_3GaC [28], where a small density of states crosses the Fermi level, and additional features are predicted about 1.5 and 2.5 eV above the Fermi level. The correspondence between the FEFF calculation and the stoichiometric Mn_3GaC data supports the supposition that the observed spectra arises from the ternary compound and is not a product of oxygen-containing impurity phases.

On the basis of this success, the FEFF model was modified in various ways in an attempt to reproduce the growth and shift in energy of the major, new feature appearing on the high energy side of the edge near 286.5 eV in the C NEXAFS spectra of the substoichiometric compounds (figure 2). Various perturbations were tried, including the simple deletion of one or more scattering carbons with or without a simultaneous contraction or expansion of the manganese around that carbon, substitution of one or more carbons with oxygen atoms, and contraction of the cluster dimensions in a manner consistent with the observed changes in crystallography and Mn K edge EXAFS data. None of these variations produced changes in the NEXAFS spectra on the same scale as those that are actually observed. For example, application of a +0.04 charge on the cluster during the FEFF calculation reproduces the experimental spectrum. Although the spectrum could be simulated by some of the variations, the resulting models are physically unlikely. For example, by assuming a combination of two carbon environments,

one with a neutral charge and one with a charge of $+0.04$ applied to the cluster during the FEFF calculation, the experimental spectrum can be qualitatively reproduced. However, this possibility is unlikely because FEFF's self-consistent potential calculation should correctly determine the charges on the various atoms in the cluster. Another perturbation that results in a good approximation of the experimental signal is a unit cell contraction approximately four times that observed in the diffraction data, a physically inconsistent value. Realistic changes in the unit cell dimensions produced insignificant changes in the calculated spectra.

Because FEFF does not elucidate the physical origins of the emerging peak at 286.5 eV, qualitative bonding and symmetry arguments based on the application of group theory were employed. In this construct, the removal of one near-neighbour carbon atom reduces the symmetry of the remaining carbon framework from octahedral O_h to a distorted cubic-type symmetry C_{4v} that breaks the carbon p orbital degeneracy. Removal of the carbon atom defines the system z-axis. The carbon p_x and p_y orbitals thus remain degenerate, with the p_z orbital energy becoming distinct. As a result of the carbon atom removal, the interatomic Mn–C bond distances perpendicular to the z-axis should remain relatively rigid, with only the Mn–C bonds along the z-axis distorting significantly. These conclusions are consistent with the observed carbon NEXAFS spectra, in which the additional peak found in the spectrum of the carbon-deficient sample grows in intensity but coexists with the original carbon peak.

As the carbon atom in the metallic perovskites is likely to be essentially neutral [21], removal of a carbon atom is not expected to perturb the valence band structure of nearby Mn or Ga, in agreement with the spectroscopic results. Evidence about the carbon sublattice is not available from x-ray diffraction data, because of the weak scattering from carbon. However, the x-ray diffraction shows no ordering (which might be observable due to a sympathetic coordinated response of the Mn and Ga sublattices to any C ordering). Also, the peaks in the x-ray diffraction patterns representing the substoichiometric materials show no significant broadening or additional structure that might occur in a material that had been subject to disproportionation or clustering. Overall consideration of the data leads to the tentative conclusion that the structure of the carbon-deficient $Mn_3GaC_{0.78}$ compound consists of complete Mn and Ga sublattices combined with an incomplete carbon sublattice of randomly dispersed carbon vacancies. The observed volume contraction of 0.46% in going from Mn_3GaC to $Mn_3GaC_{0.78}$ is consistent with the ratio of volume contraction per carbon removed that is observed in the so-called interstitial carbides such as TiC and NbC [29].

4. Discussion

Further insight into the magnetostructural transition may be gained by a review of band structure calculations focused on the electronic properties and distortions of stoichiometric Mn_3GaC and related metallic perovskites. There are no calculations of this type performed on the substoichiometric samples, and to date the problem of the FOMT in this compound remains an open question. Generally speaking, it is concluded that the character of the magnetostructural transition in Mn_3GaC is controlled by the electron density around the manganese and by the metalloid orbital hybridization [18, 23], but the specific conclusions are varied. It is reported that the conduction bands in the vicinity of the Fermi level have dominantly Mn 3d character which are non-bonding with respect to the C 2p orbitals [30, 31]. Calculations performed by Kim *et al* [32] find that the hybridization of the bands in the FM and the AFM state of Mn_3GaC are significantly different: the hybridized Ga 4p–Mn 3d band is localized in the FM state but remains delocalized in the AFM state, due to increased C 2p–Ga 4p bonding resulting from the unit cell volume decrease concurrent with the transition to the AFM state. Investigation of the valence band structure of Mn_3GaC using synchrotron-
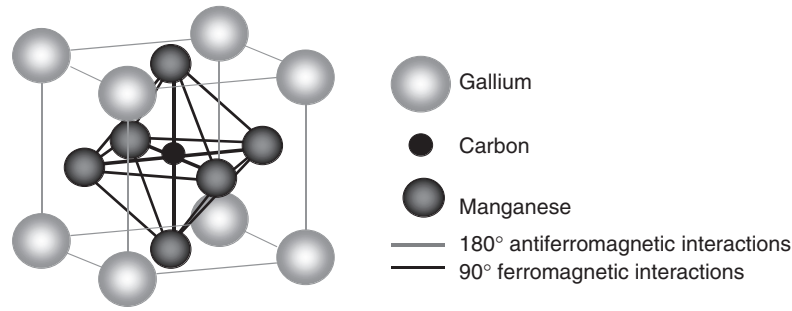
Figure 3. The stoichiometric antiperovskite Mn_3GaC unit cell with the antiferromagnetic and ferromagnetic interactions indicated.

based techniques such as x-ray magnetic circular dichroism (XMCD) and x-ray near-edge spectroscopy carried out at the Mn K absorption edge as a function of T conclude that a charge transfer from Ga to Mn occurs at the FM–AFM transition [33]. While we found no observable change in the NEXAFS spectra as a function of T through the magnetostructrual transition, the result is qualitative, and should not be considered to be inconsistent with the temperature-dependent XMCD results [24].

While illuminating, band structure calculations do not in this case provide real-space insight into the atomic and crystal defect arrangement associated with the magnetostructural transition. Real-space analysis of Mn_3GaC is provided by Goodenough [21], who employs heuristic arguments to deduce that the carbon atom in the Mn_3GaC structure is likely to be neutral, with half-filled p or s–p hybridized orbitals that can spin pair with the near-neighbour Mn e_g electrons. Complementarily, direct Mn–Mn interactions are provided by orthogonal t_{2g} electron spin correlations between Mn atoms along the edges of the Mn octahedra. Thus both direct Mn–Mn and indirect Mn–C–Mn interactions are present. Superexchange is predicted by the Goodenough–Anderson–Kanamori rules [21]. According to these rules, 180° M–ligand–M interactions, where M is a magnetic cation with partially filled d shell, are strongly AFM, whereas 90° M–M interactions are FM and much weaker. Figure 3 presents the Mn_3GaC antiperovskite structure with the AFM and FM interactions indicated. It is hypothesized here that the observed magnetostructural transitions arise from a T-dependent balance between the strongly AFM 180° Mn–C–Mn interactions and the weaker FM 90° Mn–Mn interactions that exist in Mn_3GaC. Implicit in this model is that the two exchange interactions, and hence the bond distances, must have different thermal dependences. This point may be understood by noting that the strength of the individual magnetic interactions is dependent upon the overlap integral component b_{ij} of the interatomic exchange constant J, where

$$J = -\frac{2b_{ij}^2}{U} \tag{1}$$

for half-filled cation orbitals [21]. In equation (1), U is the effective electrostatic energy needed to add an electron to an orbital and the parameter b_{ij} is a matrix element that connects two one-electron wavefunctions ϕ, located at positions R' and R with electron spin σ, and may be written as

$$b_{ij} = \int \phi_{R',\sigma} \left| \frac{p^2}{2m} + V(r) \right| \phi_{R,\sigma} \cdot d\tau \tag{2}$$

with p the electron momentum, m the electron effective mass, $V(r)$ the potential energy, and the integral is evaluated over the volume τ. The parameter b_{ij} is sensitive to small changes in

the interatomic distance; it is proportional to the orbital overlap and increases exponentially with decreasing cation–cation separation. Application of this model to the Mn_3GaC, with complete manganese, gallium and carbon sublattices, suggests that the magnetostructural transition is driven from the AFM state to the FM state by thermal expansion of the interatomic bonds to a point where the 180° Mn–C–Mn AFM interactions are overcome by the FM 90° Mn–Mn interactions. At T_t the unit cell experiences a discontinuous isotropic contraction, further strengthening the bonds. Even though the FM 90° Mn–Mn interactions are weaker than the 180° Mn–C–Mn interactions, there are many more of them and thus they contribute dominantly at the transition temperature. Experimental evidence [10] that the FOMT in Mn_3GaC is depressed with applied pressure is consistent with this model. This transition is suppressed in the carbon-deficient sample because carbon vacancies weaken the AFM correlations so that the 90° Mn–Mn FM interactions dominate the magnetic character, resulting in FM down to lowest measured T.

5. Summary and conclusions

Spectroscopic studies of the delocalized $Mn_3GaC_{1-\delta}$ (δ = 0, 0.9, 0.22) antiperovskite compound were carried out to clarify the role of carbon in its magnetic order and inherent magnetostructural transition. Room temperature carbon NEXAFS data evidenced a clear splitting of the carbon absorption bands with decreasing carbon content while the analogous metal K edges showed no changes, implying that the carbon character alone drives the transition and determines the magnetic order. A phenomenological model, based on application of the Goodenough–Anderson–Kanamori rules and consistent with the carbon spectroscopy data, attributes the magnetostructural transition found in the stoichiometric compound to a temperature-dependent imbalance in the 180° antiferromagnetic Mn–C–Mn interactions and the weak but numerous near-neighbour 90° Mn–Mn ferromagnetic interactions. This imbalance results in a first-order transition from ferromagnetism to antiferromagnetism at low temperature that is thus logically suppressed in the carbon-deficient samples.

Acknowledgments

References

[1] Hwang H-Y, Cheong S W, Radaelli P G, Marezio M and Batlogg B 1995 *Phys. Rev. Lett.* **75** 914
[2] Pecharsky V K and Gschneidner K A Jr 1997 *Phys. Rev. Lett.* **78** 4494
[3] Ullakko K, Huang J K, Kantner C, O'Handley R C and Kokorin V V 1996 *Appl. Phys. Lett.* **69** 1966
[4] Yu M-H, Lewis L H and Moodenbaugh A R 2003 *J. Appl. Phys.* **93** 10128
[5] Amos T G, Huang Q, Lynn J W, He T and Cava R J 2002 *Solid State Commun.* **121** 73
[6] Howe L and Myers H P 1957 *Phil. Mag.* **2** 554
[7] Bouchaud J-P and Fruchart R 1965 *C. R. Acad. Sci.* **261** 458
[8] Bouchaud J-P, Fruchart R, Guillot M, Bartholin H and Chaissé F 1965 *C. R. Acad. Sci.* **261** 655
[9] Bouchaud J-P, Fruchart R, Pauthenet R, Guillot M, Bartholin H and Chaissé F 1966 *J. Appl. Phys.* **37** 971
[10] Kamishima K, Bartashevich M I, Goto T, Kikuchi M and Kanomata T 1998 *J. Phys. Soc. Japan* **67** 1748
[11] Kanomata T, Kikuchi M, Kaneko T, Kamishima K, Bartashevich M I, Katori H A and Goto T 1997 *Solid State Commun.* **101** 811
[12] Fruchart D, Bertaut E F, Sayetat F and Nasr Eddine M 1970 *Solid State Commun.* **8** 91

[13] Kamishima K, Goto T, Sasaki T, Kanomata T and Inami T 2002 *J. Phys. Soc. Japan* **71** 922

[14] Kamaishima K, Goto T, Nakagawa H, Muura N, Ohashi M and Mori N 2000 *Phys. Rev.* B **63** 024426

[15] Kim W S, Chi E O, Kim J C, Choi H S and Hur N H 2001 *Solid State Commun.* **119** 507

[16] Kanomata T, Yasui H, Yoshida H and Kaneko T 1987 *J. Magn. Magn. Mater.* **70** 263

[17] l'Heritier Ph P, Boursier D, Fruchart R and Fruchart D 1979 *Mater. Res. Bull.* **14** 1203

[18] Guillot M and Pauthenet R P 1964 *C. R. Acad. Sci.* **258** 3242

[19] Kaneko T, Kanomata T and Shirakawa K 1987 *J. Phys. Soc. Japan* **56** 4047

[20] Kouvel J S 1964 *Metallurgy at High Pressures and High Temperatures* ed K A Gschneidner Jr *et al* (New York: Gordon and Breach) chapter 8

[21] Goodenough J B 1963 *Magnetism and the Chemical Bond* (New York: Interscience)

[22] Ankudinov A L, Ravel B, Rehr J J and Conradson S D 1998 *Phys. Rev.* B **58** 7565

[23] Fruchart D and Bertaut E F 1978 *J. Phys. Soc. Japan* **44** 781

[24] Uemoto S, Mauyama H, Kawamura N, Uemura S, Kitamoto N, Nakao H, Hara S, Suzuki M, Fruchart D and Yamazaki H 2001 *J. Synchrotron Radiat.* **8** 449

[25] Gamble L J, Ravel B, Fischer D A and Castner D G 2002 *Langmuir* **18** 2183

[26] Kramer M J, Yang N, Lewis L H and Moodenbaugh A R 2004 unpublished

[27] Newville M 2001 *J. Synchrotron Radiat.* **8** 322
       Ravel B IFEFFIT, Atoms, Athena, and Artemis: http://cars9.uchicago.edu/~ravel/software/, http://leonardo.phys.washington.edu/feff

[28] Shim J H, Kwon S K and Min B I 2002 *Phys. Rev.* B **66** 020406

[29] Toth L E 1971 *Transition Metal Carbides and Nitrides* (New York: Academic)

[30] Shirai M, Ohata Y, Suzuki N and Motizuki K 1993 *Japan. J. Appl. Phys.* **32/33** (Suppl.) 250

[31] Ishida S, Fujii S, Sawabe A and Asano S 1993 *Japan. J. Appl. Phys.* **32/33** (Suppl.) 282

[32] Kim I G, Jin Y J, Lee J I and Freeman A J 2003 *Phys. Rev.* B **67** 60407